https://doi.org/10.3311/PPch.37852

Periodica Polytechnica Chemical Engineering

Pervaporation Membrane Development via PSf/PMMA/PDMS Polymeric Blends and ZSM-5/TiO_2 Integration for Bioethanol Purification as Sustainable Green Energy

Tutuk Djoko Kusworo[1*], Budiyono Budiyono[1], Dani Puji Utomo[1], Kevin Setiadi Seng[1], Muhammad Itsar Hanif[1]

[1] Department of Chemical Engineering, Faculty of Engineering, Diponegoro University, Jl. Prof. Soedarto, 50275 Semarang, Central Java, Indonesia
[*] Corresponding author, e-mail: tdkusworo@che.undip.ac.id

Received: 08 July 2024, Accepted: 12 November 2024, Published online: 03 January 2025

Abstract

This study introduces a novel nanocomposite membrane designed for pervaporation (PV) by employing polymer blending, inorganic integration, and polymer coating techniques. ZSM-5 or TiO_2 nanoparticles were synthesized and incorporated into a polysulfone (PSf) and poly(methyl methacrylate) (PMMA) matrix, followed by a coating of polydimethylsiloxane (PDMS) to enhance perm-selectivity. Comprehensive analyses confirmed the well-dispersed nature of the nanoparticles and a significant increase in hydrophilicity. The research systematically examined the effects of particle loading, PDMS coating, and temperature on the separation efficiency. The findings revealed that the PDMS-coated PSf/PMMA/ZSM-5 membrane with a 2 wt.% loading demonstrated a substantial 41% increase in permeate flux and achieved a separation factor of 61.227 ± 1.92 at 40 °C. These improvements are attributed to the establishment of water channels and the molecular sieving effect introduced by the ZSM-5 incorporation. This study suggests that the developed membrane offers promising enhancements for ethanol recovery through pervaporation, showcasing the potential of nanocomposite membranes in improving separation efficiency and selectivity.

Keywords

bioethanol, green energy, nano-composite membrane, pervaporation, selectivity

1 Introduction

The global population is consistently increasing [1], leading to a surge in energy demand and consumption due to improved living standards [2]. Projections indicate a 48% rise in global energy demand between 2012 and 2040 [3]. Historically, fossil fuels such as petroleum, coal, and natural gas have been the primary energy sources, particularly since the industrial revolution of the 19th century [4]. The advent of the internal combustion engine further intensified the demand for petroleum towards the end of the 19th century. Presently, fossil fuel consumption surpasses 1.2 million TWh, with expectations of continued growth [5]. Despite the efficiency and quality controls in thermal power plants, increased fossil fuel consumption has led to environmental challenges, as extensively studied [6]. These issues encompass global warming and air pollution, impacting public health and prompting global concerns about fossil fuel depletion, urging a shift towards renewable energy sources.

The late 20th century witnessed a heightened interest in biofuels as a viable alternative to fossil fuels [7]. Among these biofuels, bioethanol has emerged as a significant plant-based fuel, utilized either directly or as a fuel additive [8]. Recent research has also emphasized that the economic value of bioethanol can be augmented by producing it from waste materials [9]. Bioethanol presents advantages such as reduced greenhouse gas emissions, lower carbon monoxide emissions, and the potential to mitigate global warming [10]. However, the production of high-purity bioethanol is crucial, requiring advanced separation methods due to the limitations of traditional distillation processes and the need for high ethanol purity as biofuel usage [11]. To address the substantial energy consumption associated with azeotropic distillation, membrane technology is considered an energy-efficient alternative [12]. Membranes act as selective barriers, separating components based on molecular size, electrostatic

Cite this article as: Kusworo, T. D., Budiyono, B., Utomo, D. P., Seng, K. S., Hanif, M. I. "Pervaporation Membrane Development via PSf/PMMA/PDMS Polymeric Blends and ZSM-5/TiO_2 Integration for Bioethanol Purification as Sustainable Green Energy", Periodica Polytechnica Chemical Engineering, 2025. https://doi.org/10.3311/PPch.37852

charge, polarity, and solid diffusivity. Among membrane processes, pervaporation (PV) stands out as a promising method for bioethanol separation to obtain anhydrous ethanol [10]. PV is an energy-efficient membrane separation process that integrates permeation and evaporation to selectively extract components from liquid mixtures using a dense polymeric membrane. In this process, the liquid mixture comes into contact with one side of the membrane, while the resulting vapor (pervaporate) is collected and condensed [13]. PV employs a non-porous and asymmetric membrane, dividing the feed into permeate and retentate streams, making it suitable for overcoming the azeotropes limitation in conventional distillation [14].

PV holds potential as a substitute for traditional distillation methods, offering environmental safety and cost-effectiveness compared to the latter. Nonetheless, PV faces challenges such as limited selectivity, membrane fouling, high costs, and the necessity for optimal operating conditions [15]. Prospects for future success in pervaporation lie in advancements in membrane technology, refining the process through optimization, integrating with other separation techniques, exploring new applications, and establishing sustainable procedures. By surmounting these hurdles and capitalizing on these opportunities, pervaporation can enhance its efficacy, broaden its applicability, and minimize its environmental impact. Common membrane materials include natural and synthetic hydrophilic polymers, as well as inorganic polymers. Recently, organic-inorganic hybrids and layer-by-layer assembled membranes have gained significant attention [16]. Nanocomposite membranes have been substantially studied as the advanced polymeric membrane material of PV process. Membrane materials including polydimethylsiloxane (PDMS), chitosan, alginate, polyvinyl fluoride (PVDF), polysulfone (PSf), and alginate have been extensively investigated over time due to their capacity to offer effective separation outcomes and reliable processing techniques [12, 17, 18]. Among these polymers, PSf stands as promising basic material due to its stability and compatibility with many nanoparticle fillers. For improving the membrane characteristics, polymer blends are commonly used to prepare membrane for PV. Poly(methyl methacrylate) (PMMA), recognized for its high Young's modulus and hardness, exhibits exceptional physical and mechanical properties, positioning it as a promising candidate for enhancing thermal resistance and compatibility in polymer blends [19]. Zainol Abidin et al. [20] revealed the improved separation performance of PSf and PMMA blended membrane. Furthermore, the incorporation of inorganic nanofillers also have been studied to investigate the membrane properties and diffusion behavior. In this regard, Sardarabadi et al. [21] reviewed the effects of nanofillers on the properties of membrane in PV process. They concluded that the addition of nanoparticles into polymeric membrane provided significant improvement in both selectivity and permeability. Among the studied inorganic fillers, hydrophobic zeolites have garnered significant attention from researchers for their application in ethanol recovery through PV. A membrane based on ZSM-5 demonstrated selectivity towards ethanol, attributed to its hydrophobic nature and low Al content. In the study by Weyd et al. [22], ZSM-5 membranes deposited on a support structure consisting of a titania tube and three intermediate ceramic titania layers exhibited exceptionally favorable separation performance. This included permeation flux values ranging from 810 to 11,300 g m^{-2} h^{-1} and separation factors between 49.9 and 97.7 for enriching ethanol from around 5 wt.% aqueous solutions, across a temperature range of 40 to 120 °C. Titania is a versatile nanomaterial employed in catalysis, photocatalysis, and antibacterial applications valued for its biocompatibility, low cost, and chemical stability. TiO_2 also improves ion dynamics in PMMA-based gels, and its large surface area enhances interaction between devices and fluids, essential for optimal membrane performance [23].

Despite the lag in the development of nanocomposite membranes for bioethanol dehydration in the PV process, researchers are actively exploring novel membrane materials with superior characteristics and performance. In this study, PV membranes were developed and investigated through the polymer blending of PSf/PMMA and the incorporation of ZSM-5/TiO_2. Additionally, surface modification via PDMS coating was employed to enhance the separation performance of the membrane and increase the concentration of ethanol. To the best of our knowledge, there are limited studies involving polymeric blends and the incorporation of inorganic fillers to develop innovative PV membranes. By introducing this hybrid strategy that leverages the benefits of both organic and inorganic components, this study not only overcomes the challenges faced by traditional membranes but also provides a sustainable and cost-effective solution for bioethanol purification. Ultimately, this research bridges gaps in the literature and contributes to the advancement of renewable energy sources, demonstrating the potential of innovative membrane technology to achieve higher efficiency in the PV process.

2 Materials and methods

2.1 Materials

The materials and reagents used in this research included cetyltrimethylammonium bromide (CTAB, 10.7 wt.%) that was purchased from Sigma-Aldrich. Chemical reagents such as tetraethyl orthosilicate (TEOS, 6.25 mL), Aluminum iso-propoxide, NaOH, polydimethyl siloxane (PDMS), N-methyl-2-pyrrolidone (NMP), titanium (IV) isopropoxide (TiPP), acetic acid, ethanol were acquired from Merck, Singapore. Materials for pervaporation membrane fabrication: polysulfone was purchased from Advanced Material, US. Meanwhile, PMMA was purchased from HiMedia, India. Deionized (DI) water was utilized for aqueous solution preparation in the whole experiment.

2.2 Synthesis of ZSM-5 or TiO_2 nanoparticles

The initial step for preparing ZSM-5 involved mixing 6.25 mL of TEOS, 10 mL of CTAB (10.7 wt.%), and 1.5 mL of 1 M NaOH solution. Aluminum isopropoxide was then added at room temperature, and the mixture was stirred for 8 h. This blend was transferred to a 50 mL stainless steel autoclave and heated to 150 °C using an oil bath. The product was subsequently dried at room temperature and calcined at 550 °C for 4 h to produce nanocrystal ZSM-5. For the synthesis of TiO_2 nanoparticles, 30 mL of TiPP, 6 mL of acetic acid, and 39 mL of ethanol were mixed and stirred until a homogeneous solution was formed. The resulting sol was then calcined for 3 h at 450 °C, yielding TiO_2 nanoparticles.

2.3 Fabrication of PDMS-coated PSf/PMMA/ZSM-5/TiO_2 membrane

The subsequent stage involves preparing a composite membrane of PSf, PMMA, PDMS, TiO_2, and ZSM-5 as presented in Table 1. The membrane fabrication process utilizes dry-wet phase inversion, followed by the dip-coating method. The manufacturing process initiates by preparing PSf and PMMA polymers at concentrations of 15% and 5%, respectively, dissolving each polymer in NMP. The resulting solutions are stirred vigorously for 24 h. ZSM-5 or TiO_2 are suspended in a solvent through ultrasonication at 20 kHz for 30 min, and then the mixture is combined with the polymer solution. This combined solution is cast onto clean glass plates to create a membrane with a thickness of 150 μm. The film is subsequently immersed in DI water for 24 h. The resulting membrane is then dried in an oven at 60 °C for 24 h. After drying, the membrane is soaked in ethanol for 24 h, followed by immersion in a PDMS solution for 5 min and subsequent drying in an oven at 60 °C for an additional 24 h. The scheme of the preparation of membranes is illustrated in Fig. 1.

Table 1 Composition of fabricated membranes

Membrane	PSf (wt.%)	PMMA (wt.%)	ZSM-5 (wt.%)	TiO_2 (wt.%)	PDMS (wt.%)
PP0	15	5	0	-	-
PPZ1	15	5	1	-	-
PPZ1.5	15	5	1.5	-	-
PPZ2	15	5	2	-	-
PPT1	15	5	-	1	-
PPT1.5	15	5	-	1.5	-
PPT2	15	5	-	2	-
S-PPZ	15	5	2	-	4
S-PPT	15	5	-	2	4

2.4 Characterization of the PDMS-coated PSf/PMMA-ZSM-5/TiO_2 membrane

The morphological characteristics of the fabricated membranes were analyzed using a scanning electron microscope (SEM, JEOL Series JSM-6510-LA, Japan) equipped with energy dispersive X-ray (EDX) for elemental composition and mapping analysis. The identification of functional groups in native ZSM-5, TiO_2, and organic materials was conducted using Fourier-transform infrared spectroscopy (FTIR, Perkin Elmer Frontier, USA). The phase crystallinity of the materials was assessed through X-ray powder diffraction (XRD, X-Ray Diffraction SHIMADZU XRD-7000, Japan) with Cu Kα irradiation at 0.15405 nm, covering a diffraction angle 2θ range from 5 to 80°. The mechanical strength of the membranes was assessed using a UTS H001 testing machine (China), measuring tensile strength and elongation at break. A square membrane sheet (5 × 5 cm^2) was clamped in a sample holder and stretched at a rate of 20 mm min^{-1}.

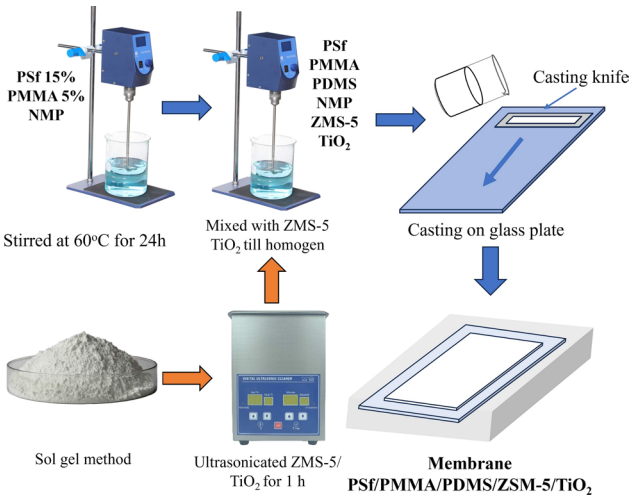

Fig. 1 Scheme of the preparation of membranes

2.5 Membrane performance evaluation

The transport properties of fabricated nanocomposite membranes were examined for the pervaporation dehydration of ethanol with initial concentration of 70 wt.% in water at 22 °C. The experiments were conducted in a steady-state circulated cell with an effective membrane area of 19.63 cm^2. The permeate side pressure was monitored using a pressure gauge, as shown in Fig. 2, and was maintained at a downstream pressure of less than 13.332 Pa throughout the experiments. This real-time monitoring enabled effective evaluation of membrane performance during pervaporation and assessment of the impact of operating conditions on permeate flux and separation efficiency. The schematic of the pervaporation setup is illustrated in Fig. 2.

The performance of PPZ- and PPT-based membranes is evaluated based on various parameters including permeation flux (J_i), component permeability (P_i^G), membrane selectivity (α), separation factor (β), and pervaporation separation index (PSI).

$$J_i = \frac{V_i}{A \times t} \tag{1}$$

Component permeability, typically expressed in barrers (1 barrer = 1 × 10^{-10} cm^3 (MPa) cm/cm^2 s cmHg), is calculated using Eq. (2):

$$P_i^G = J_i \frac{\gamma}{P_{i_f} - P_{i_p}} \tag{2}$$

where V_i is the volume of permeated component (L), A is the effective membrane area (m^2), t is the permeation time (h), γ is the membrane thickness (cm), P_{i_f} and P_{i_p} are the partial vapor pressure of component i on the feed and permeate side of the membrane, respectively.

Membrane selectivity (α), defined as the ratio of component permeabilities, is calculated as:

$$\alpha = \frac{P_i^G}{P_j^G} \tag{3}$$

where P_i^G and P_j^G are the component permeabilities.

The separation factor (β) is calculated using Eq. (4):

$$\beta = \frac{y_e / y_w}{x_e / x_w} \tag{4}$$

where y_i and y_j are the mass fractions of components i and j, respectively, in the permeate; x_i and x_j are the mass fractions of components i and j, respectively, in the feed.

PSI is calculated as

$$\text{PSI} = J \times (\beta - 1) \tag{5}$$

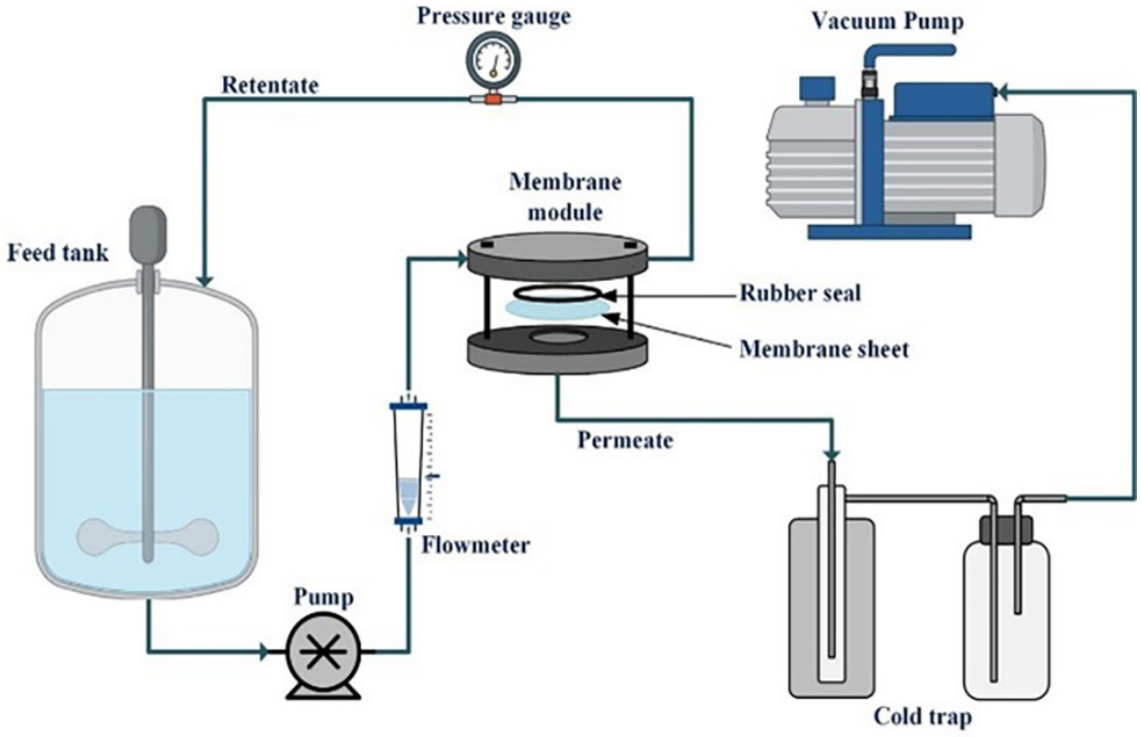

Fig. 2 Membrane pervaporation process equipment set

PSI is the pervaporation separation index (kg m^{-2} h^{-1}). The concentration of ethanol in permeate and feed were analyzed using gas chromatography (Shimadzu NEXIS GC–2030) with a polar column, such as the SH-Rxi-5Sil MS or SH-Rtx-Wax columns. Pervaporation experiments for each membrane were conducted at least three times, and the average values of the parameters were calculated for analysis.

3 Results and discussion

3.1 SEM analysis for morphological properties

Morphological analysis of membranes is a crucial aspect to ensure the overall quality of the membrane, impacting both membrane permeability and selectivity. The observation of membrane morphology using SEM aims to discern the characteristics of a membrane, both from its surface cross-section and its transverse section [24]. The surface and cross-sectional morphologies of S-PPZ and S-PPT membranes were observed by SEM as shown in Fig. 3. The surface morphology of S-PPZ and S-PPT membranes incorporated with inorganic fillers ZSM-5 nanocrystals and TiO_2 nanoparticles respectively appears smooth and dense, with several white spots on the membrane surface, attributed to the embedded of ZSM-5 nanocrystals and TiO_2 nanoparticles. SEM analysis revealed that the synthesized TiO_2 nanoparticles have an average size of 42 nm. In pervaporation membranes, these nanoparticles can improve flux and selectivity by enhancing hydrophilicity and reducing fouling. The emergence of these white spots is likely due to the high affinity between ZSM-5 nanocrystals and TiO_2 nanoparticles within the PSf/PMMA matrix. Fig. 3 (a) indicates the presence of ZSM-5 nanocrystal agglomerates on the membrane's surface, displaying a morphology resembling flowers surrounded by irregular white shapes [25]. This can be attributed to the phase transformation between the membrane and ZSM-5, as nanocrystals possess a high surface energy, causing them to agglomerate [26]. Additionally, the agglomeration of ZSM-5 nanocrystals can occur due to their migration from the membrane matrix, driven by solvent and non-solvent exchange during phase inversion, causing nanoparticles to accumulate on the membrane's surface [27]. Meanwhile,

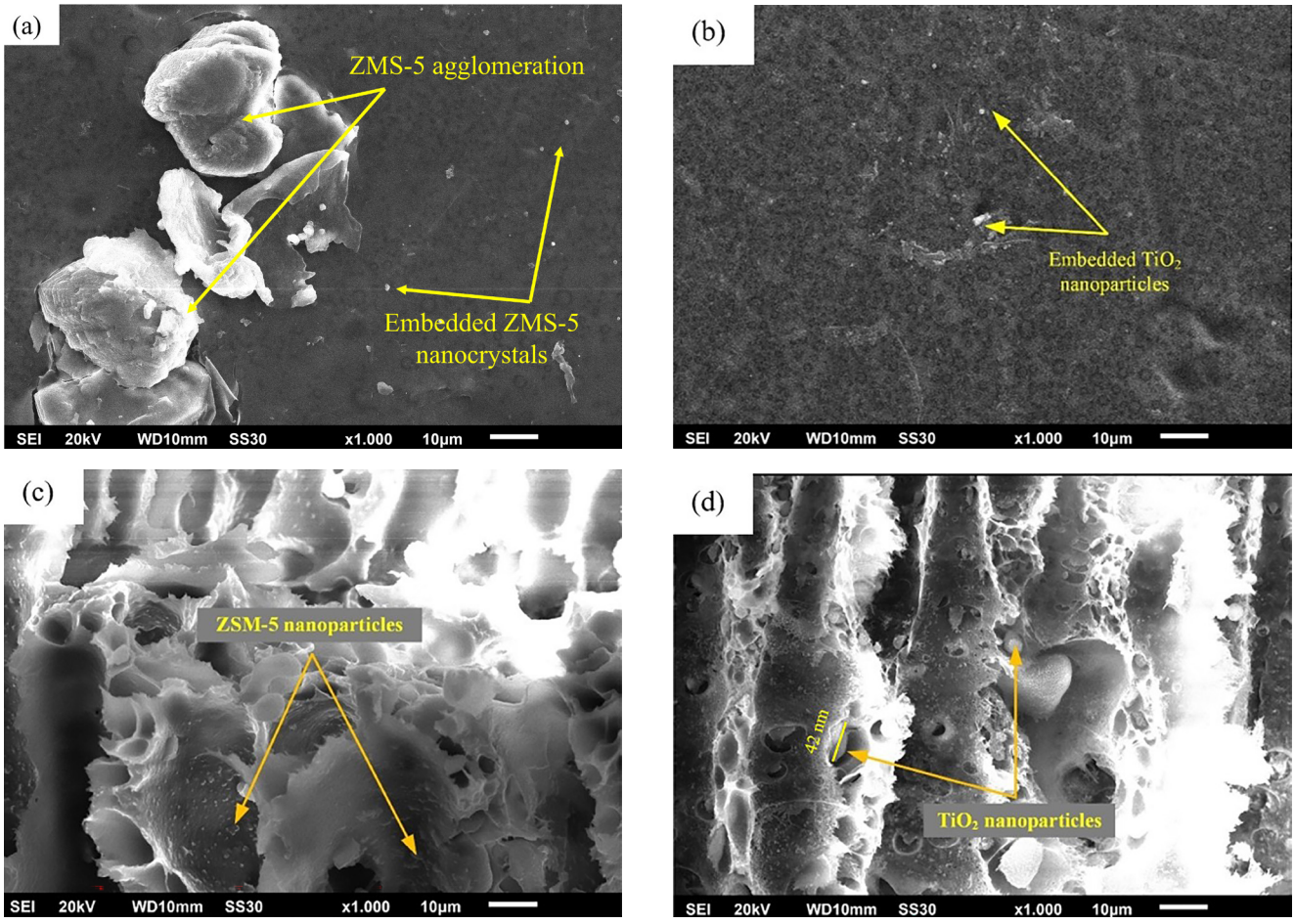

Fig. 3 SEM images of (a) surface section of the S-PPZ membrane; (b) surface section of the S-PPT membrane; (c) cross-section of the S-PPZ membrane; (d) cross-section of the S-PPT membrane (images at ×1000 magnification)

in Fig. 3 (b), the surface morphology of S-PPT membrane exhibits smooth surface without nanoparticle agglomerates, suggesting that TiO_2 nanoparticles are well attached and owing excellent chemical compatibility with the polymers [27]. There is no sign of phase separation in both S-PPZ and S-PPT membranes, indicating a complete interaction between PSF/PMMA and ZSM-5; TiO_2 and shows good compatibility between the two moieties.

3.2 EDX analysis for elemental composition and distribution

The evaluation of elemental composition and distribution was performed using EDX analysis as presented in Fig. 4. The elemental mapping using EDX revealed the distribution of carbon, oxygen, sulfur, and silicon on the surface of the membranes. The pervaporation membranes S-PPZ and SPPT exhibited dense and uniform distribution of C, O and S atoms as the main elements of PSf and PMMA molecules blended through the mixing method. The high concentration of Si indicates the presence of PDMS layer on the membrane surface. As depicted in Fig. 4 (a) and (c), agglomerates of ZSM-5 nanocrystals were identified, indicated by the red nodules consisting of Al, Na, and Fe in the EDX mapping image. The finding was further confirmed by SEM analysis, displaying the presence of ZSM-5 nanocrystal agglomerates in the surface structure of the S-PPZ, as shown in Fig. 4 (a). Additionally, the K alpha peak of aluminum was detected, indicating the dispersion of ZSM-5 within the composite membrane. Subsequently, elemental mapping analysis within the S-PPT membrane is presented in Fig. 4 (b) and (d). The EDX results in the S-PPT membrane showed two types of Ti peaks, K alpha and K beta, indicating the presence of TiO_2 within the composite membrane. However, the measured mass composition of Ti was only 0.48 wt.% (0.8 wt.% as TiO_2), which was lower than the initial membrane fabrication formula i.e., 2 wt.%. This

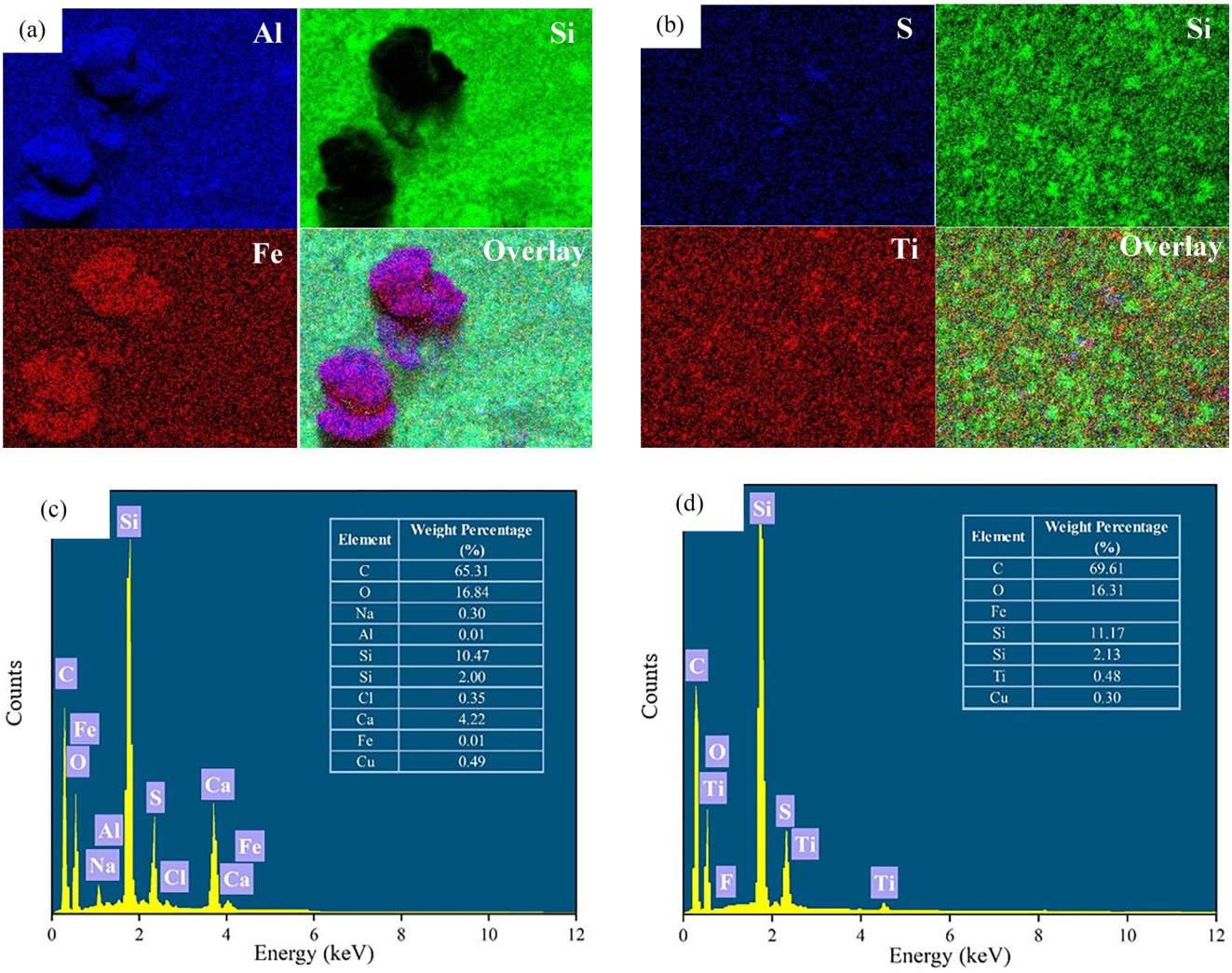

Fig. 4 SEM-EDX analysis results: (a) elemental mapping of S-PPZ membrane; (b) elemental mapping of S-PPT membranes; (c) EDX spectra of S-PPZ membrane, (d) EDX spectra of S-PPT membrane

discrepancy may have occurred due to the leaching of TiO_2 nanoparticles during phase inversion [28], resulting in a mismatch between the measured value and the initial membrane formula. Nevertheless, this analysis further confirms the successful combination of PSf/PMMA blend, TiO_2 and ZSM-5 incorporation, and PDMS coating as composite pervaporation membranes for bioethanol dehydration.

3.3 AFM analysis of fabricated membranes

AFM analysis is an essential characterization in membrane preparation for evaluating the surface roughness of membranes because it can provide in-depth information about the microscopic structure and surface topography of the membrane. In this study, AFM was employed to ensure that both membranes have the appropriate surface roughness for application in pervaporation processes.

Based on Fig. 5, the average roughness (Ra) values for the S-PPZ and S-PPT are 13.884 ± 1.73 nm and 10.872 ± 2.18 nm, respectively. A higher surface roughness level signifies increased surface porosity of the membrane and an expanded range of substrate pore sizes for PDMS coated PSf/PMMA [29]. Additionally, the decrease in surface roughness has been reported to have lower water contact angle value [30]. This is because an increase in surface roughness reduces the membrane's ability to resist water, leading to a lower contact angle [31]. Lou et al. [32] stated in their research that the addition of hydrophilic additives like ZSM-5 or TiO_2 can enhance the hydrophilic properties of the membrane, as evidenced by a decrease in the contact angle. This is attributed to the fact that the addition of hydrophilic

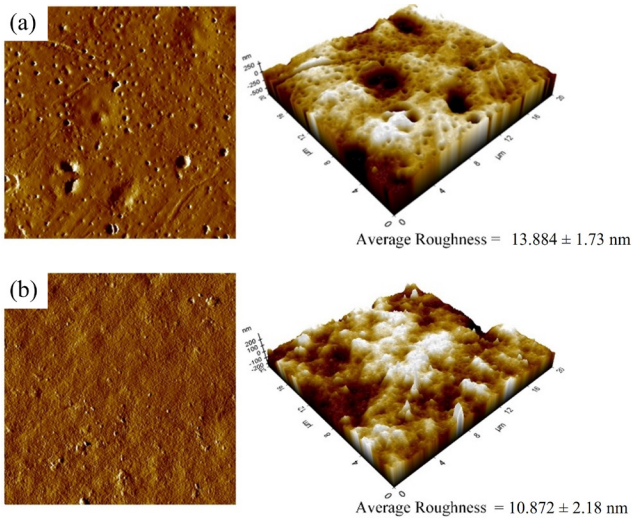

Fig. 5 AFM surface topologies of (a) S-PPZ membrane and (b) S-PPT membrane

nanoparticles can increase the surface roughness of the membrane, thus providing better contact between water and -OH groups, leading to diffusion through the membrane surface. In this study, a hydrophilic pervaporation system was used, where water diffuses through the semi-permeable membrane to become the permeate.

3.4 XRD and FTIR analysis of fabricated membranes

XRD analysis is commonly used to identify changes in the crystallinity materials. Beyond its primary function of identifying crystalline phases, this non-destructive analysis also proves valuable for detecting the presence of various materials [27]. In this study, XRD pattern tests were conducted on ZSM-5 nanocrystals, TiO_2 nanoparticles, S-PPZ, and S-PPT membranes. The results of the XRD pattern analysis are presented in Fig. 6 (a). The crystallinity of the membrane also plays a role on its performance. The presence of ZSM-5 nanocrystals and TiO_2 nanoparticles in the composition of the nanohybrid membrane increased the membrane crystallinity, resulting in a more regular arrangement of the polymer and denser membrane. The S-PPZ membrane exhibits a sharp crystalline peak that analogous with ZSM-5 nanocrystals, resembling the presence of crystalline ZSM-5 in polymer matrix. This suggests that ZSM-5 has successfully dispersed into the PSf/PMMA polymer with PDMS coating. On the other hand, there are two broad peaks observed at 2θ position of 12.12° and 17.95°, indicating the presence of amorphous characteristics of polysulfone and polymethyl methacrylate in the membrane [33, 34]. The blending of two or more polymers in polymerization can induce changes in the broad diffraction pattern shifts observed in the material [35]. Meanwhile, XRD analysis of the nanohybrid S-PPT membrane also shows peaks corresponds to the crystalline XRD pattern of anatase TiO_2. It indicates that TiO_2 has successfully combined with the PSf/PMMA/PDMS membrane. Furthermore, it suggests that there is good interaction between the TiO_2 nanoparticles and the blended polymer PSf/PMMA with PDMS coating. The crystalline peaks are found at 2θ values of 27.51°, 36.24°, 41.29°, 54.29°, and 56.81°. Moreover, the peaks are attributed to the (110), (101), and (200) planes, confirming the existence of the rutile TiO_2 phase [36]. However, some crystalline peaks in the S-PPT membrane are not as distinct as the crystalline peaks in the TiO_2 nanoparticles. This may be due to the leaching of TiO_2 nanoparticles during the phase inversion process, resulting in some less distinct peaks [28]. Like the S-PPZ membrane, the

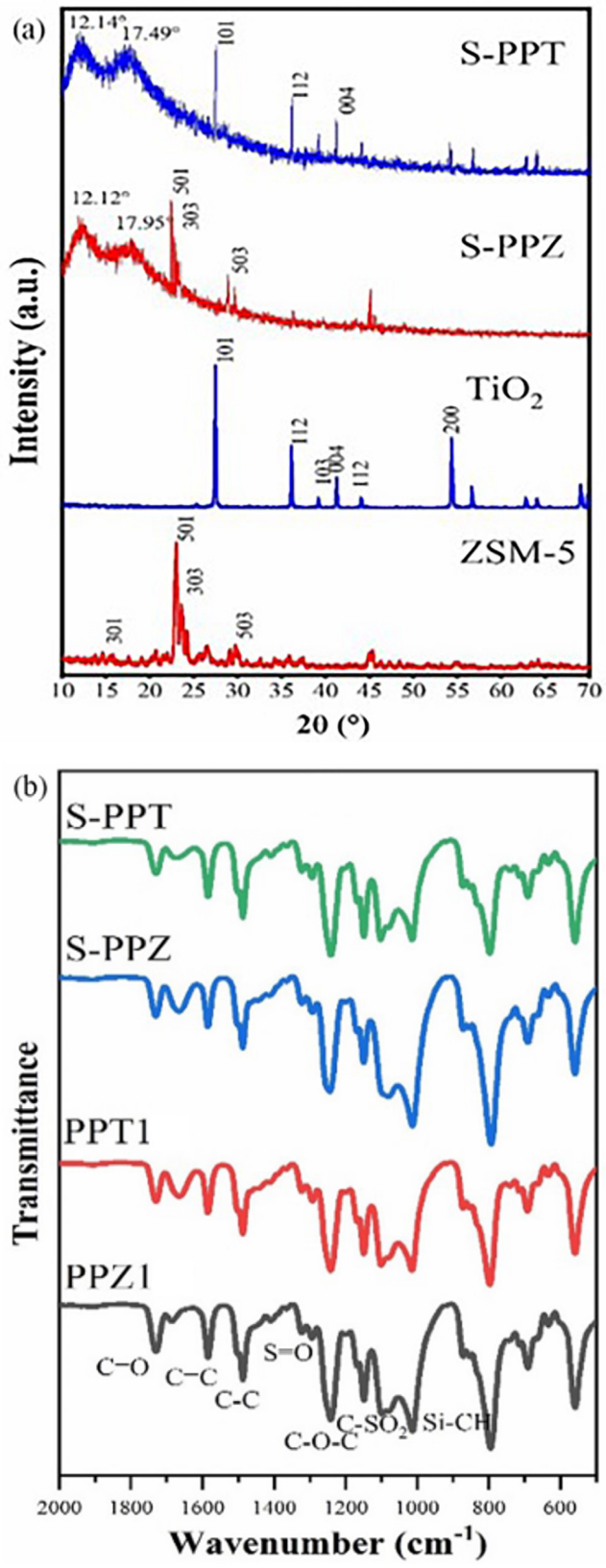

Fig. 6 (a) XRD pattern of S-PPZ and S-PPT PV membranes and their respective inorganic fillers; (b) FTIR spectra of PPZ1; PPT1; S-PPZ; and S-PPT membranes

S-PPT membrane also exhibits two broad peaks indicating amorphous characteristics resulting from the polymer blending of PSf and PMMA. This characterization implies that incorporating and dispersing ZSM-5 nanocrystals and TiO_2 nanoparticles into the PSf/PMMA with PDMS coating has the potential to improve the properties and overall performance of the membrane.

Fig. 6 (b) shows the FTIR spectra of PPZ1, PPT1, S-PPZ, and S-PPT membranes. It can be seen that there are no significant differences in the FTIR spectra of the four tested membrane structures, indicating no significant changes in the polymer backbone. The characteristic peaks of polysulfone, such as C-SO_2-C, C-O-C, S=O, CH_3-C-CH_3, and C=C, are evident. Additionally, weak C-H sp^3 functional group peaks are observed. The addition of ZSM-5 nanocrystals and TiO_2 nanoparticles introduces new spectra with intense and broader peaks around 1672 cm^{-1}, indicating Si-OH bonds in ZSM-5 and Ti-OH bonds in TiO_2. These bonds lead to stronger dipole-dipole interactions with water, increasing the surface hydrophilicity of both membranes. In the FTIR spectrum, the region below 800 cm^{-1} shows multiple peaks, indicating lattice bending and vibration. These peaks correspond to functional groups like Si-O-Si and Al-O-Si in ZSM-5, reflecting the zeolite's crystal structure. The presence of these peaks suggests interactions, such as hydrogen bonding or ionic interactions, which may affect the membrane's mechanical properties and stability. The complexity of the ZSM-5/TiO_2 polymer blend leads to various vibration modes, offering insights into the molecular interactions and phase behaviors important for evaluating membrane performance.

3.5 Water contact angle and tensile strength

The modification of PSf/PMMA blended membranes with the addition of ZSM-5 nanocrystals and TiO_2 nanoparticles has a significant impact on membrane hydrophilicity, as evidenced by the value of water contact angle in Table 2. The addition of 1 wt.% ZSM-5 nanocrystal to the PSf/PMMA blended membrane decreases the water contact angle value from 82.2° to 63.50°. Similar effects are observed with the addition of 1 wt.% of TiO_2 nanoparticles to the PSf/PMMA blended membrane where the reduction of the contact angle value from 82.20° to 74.77° was observed. Research by Lou et al. [32] indicates that the addition of hydrophilic additives such as ZSM-5 or TiO_2 can enhance membrane hydrophilicity, as evidenced by the reduced contact angle value. This result is attributed

Table 2 Water contact angle and mechanical strength of fabricated membranes at 50 °C

Membrane	Contact angle (°)	Tensile strength (MPa)	Youngs modulus (MPa)	Elongation break (%)
PP	82.20 ± 2.31	21.37 ± 1.60	4.48 ± 1.65	4.77 ± 1.71
PPZ1	63.50 ± 1.13	24.58 ± 2.18	6.32 ± 2.03	3.89 ± 1.99
PPT1	74.77 ± 2.02	23.21 ± 2.37	5.69 ± 2.15	4.08 ± 0.83
S-PPZ	83.30 ± 1.87	25.42 ± 1.19	4.88 ± 1.56	5.21 ± 2.15
S-PPT	85.90 ± 1.55	25.11 ± 0.98	5.16 ± 1.15	4.87 ± 1.12

to the increase in surface energy caused by hydrophilic nanoparticles incorporation, facilitating better affinity between membrane and water molecules and allowing for greater diffusion through the membrane surface. This is further supported by the study conducted by Xu et al. [37], where nanoparticles increased membrane hydrophilicity due to their high surface energy, enhancing the absorption of water molecules on the membrane surface. The S-PPZ and S-PPT membranes possessed contact angle values of 83.3° and 85.90°, which are higher than those of uncoated membranes (PP, PPZs, and PPTs). It could be due to the hydrophobic nature of PDMS coating layer. Furthermore, the S-PPZ membrane has lower contact angle than that of S-PPT, suggesting that ZSM-5 nanocrystals exhibit higher hydrophilicity than those of TiO_2 nanoparticles. These results align with the SEM cross-section characterization of the S-PPZ membrane in Fig. 3, where macro-voids are observed in the polymer sublayer. These macro-voids enhance the membrane's water absorption capacity. This characterization shows that the modified membranes exhibit a more hydrophilic nature compared to the pristine membrane, consequently resulting in an increase in water molecule permeability.

The permeance of water and bioethanol increased with temperature due to enhanced molecular mobility and vapor pressure, with water showing a more pronounced rise because of its smaller size and higher volatility. Membranes with TiO_2 nanoparticles exhibited a greater improvement, attributed to their enhanced hydrophilicity and reduced fouling, boosting water transport without significantly affecting bioethanol selectivity.

The mechanical properties play a crucial role in assessing the stability of the developed membranes for pervaporation applications. The tensile strength and elongation break of the fabricated membranes were presented in Table 2. Mechanical strength and elongation at break are not necessarily directly proportional. This observation is likely influenced by the modification of the membrane through the addition of ZMS-5 and TiO_2. ZMS-5's structure enhances the affinity between the filler and the polymer, improving the membrane's mechanical strength. This strong interaction also increases the membrane's resistance to fracture under tensile stress, resulting in greater elongation at break. As discussed in the previous section that ZSM-5 or TiO_2 have good compatibility with PSf/PMMA blended polymer, the mechanical properties of the nano-composite membranes are significantly enhanced. The incorporation of 1 wt.% of ZSM-5 and TiO_2 increased the tensile strength from 21.37 to 24.58 and 23.21 MPa, respectively with slightly decrease of elongation break. This clearly shows that the mechanical strength of the membrane is influenced by the interaction of the ZSM-5 or TiO_2 with PSf/PMMA matrix. The PDMS coating on the nano-composite membrane also slightly increased both tensile strength and elongation break. Specifically, the increase in tensile strength and elongation at break can be attributed to the entanglement between the PSf/PMMA reinforcing phase and the flexible long-chain siloxane, along with the PDMS matrix, contributes to stress dissipation [38]. All modified membranes have demonstrated improved mechanical strengths and are well-equipped to withstand the applied vacuum during pervaporation experiments.

3.6 Pervaporation performance evaluation

The evaluation of membrane performance for bioethanol purification was conducted using a binary system of ethanol and water. In Fig. 7, the increase in ethanol concentration over time was examined for various types of nano-composite membranes. Fig. 7 (a) illustrates the impact of adding ZSM-5 to the PSf/PMMA blended membrane. All membranes incorporating ZSM-5 exhibited higher ethanol concentrations compared to the native PSf/PMMA membrane. The maximum ethanol concentration achieved was approximately 78% with a 2 wt.% ZSM-5 loading concentration (PPZ2). The enhancement in ethanol concentration can be attributed to the increased hydrophilicity of the membrane, resulting in improved water permeability through the membrane barrier. ZSM-5, known for its molecular sieving properties, facilitates the separation of ethanol and water [39]. Fig. 7 (b) demonstrates the increase in bioethanol concentration with the addition of TiO_2. The highest bioethanol concentration reached was 76.5 wt.% with the PPT2 membrane. TiO_2 addition

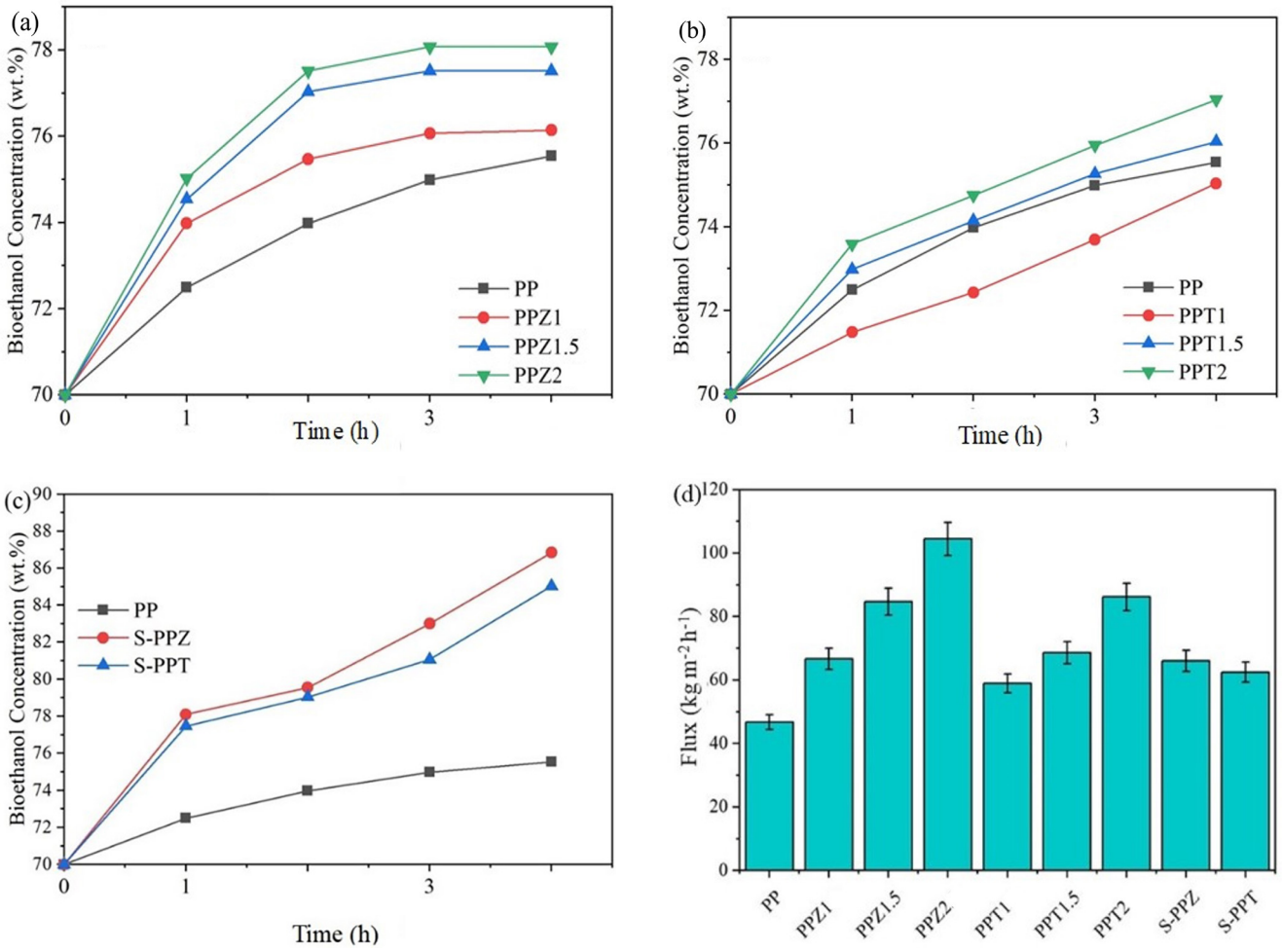

Fig. 7 Profile of bioethanol concentration as function of operating time for (a) ZSM-5 loaded membrane, (b) TiO_2 loaded membrane, and (c) PDMS coated membrane, respectively; (d) total flux of the fabricated membranes

enhanced the membrane's hydrophilicity, as indicated by FTIR spectrum and water contact angle analysis, leading to an increased water flux. Thus, a ZSM-5 or TiO_2 loading concentration of 2 wt.% yielded the highest bioethanol concentration. The PDMS coating on the membrane surface significantly improved bioethanol concentration, with S-PPZ membrane achieving the highest result at 87%, followed by S-PPT membrane at 85%. The PDMS layer aided in restoring defects caused by nanofiller agglomeration in the membrane matrix. He et al. [40] reported that a PDMS-coated membrane could enhance separation performance by up to 30% with higher ethanol recovery. The overall permeate flux, depicted in Fig. 7 (d), demonstrated that the total flux of PSf/PMMA with 2 wt.% ZSM-5 loading reached the highest value at 104.426 kg m^{-2} h^{-1}, approximately 2.2 times higher than the native PSf/PMMA blended membrane. Similar patterns were observed for TiO_2-incorporated membranes, with the highest total flux achieved at 86.163 kg m^{-2} h^{-1} (1.8 times higher than the control membrane) for PPT2. Notably, when the loading level was below 2 wt.%, the newly formed voids/diffusion paths near the interface of particles and polymer matrix were insufficient to significantly enhance membrane permeability. However, the slight decrease in total flux due to PDMS coating is deemed acceptable as long as the improvement in separation efficiency is remarkably significant.

3.7 Separation factor and pervaporation separation index

In addition to membrane modifications, operational parameters such as temperature play a crucial role in influencing separation performance. Fig. 8 illustrates the separation factor (β) and pervaporation separation index of SPPZ and S-PPT membranes, revealing a tendency for both parameters to decrease at elevated temperatures. This observed trend in the separation factor can be attributed to

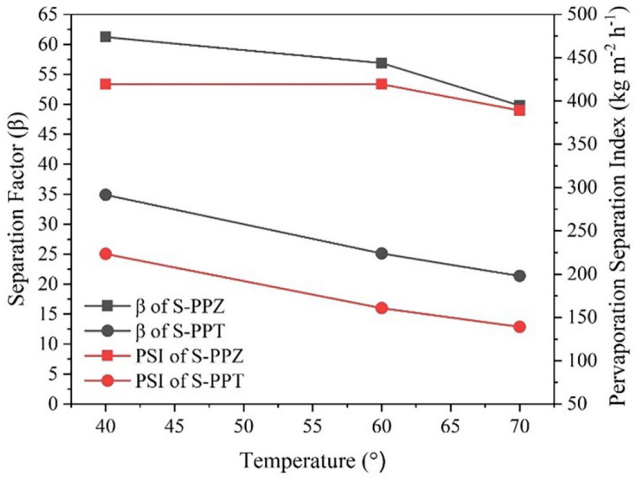

Fig. 8 Separation factor and pervaporation separation index of S-PPZ and S-PPT at different operating temperature

the preferential adsorption of ethanol and the swelling of PDMS induced by temperature [41]. Temperature-induced PDMS swelling creates additional diffusion paths for molecules, resulting in a higher flux. However, this enhanced diffusion path initially impacts ethanol diffusion, leading to a lower separation factor in high-temperature systems. In essence, temperature affects the transport behavior of permeates and the polymer chain swelling within the membrane structure. Higher temperatures elevate the frequency and amplitude of segmental motion in a polymer chain, increasing the volume of empty space and decreasing the degree of swelling in the polymer matrix within the membrane structure. The expanded empty volume provides room for permeate displacement, and the increased vapor pressure of permeate molecules at higher temperatures, in combination with these factors, leads to heightened flux and diminished separation factor.

The S-PPZ and S-PPT membranes exhibited their highest separation factors at 61.227 ± 1.92 and 34.893 ± 2.21, respectively, with both measurements taken at 40 °C. Meanwhile, the maximum PSI values for the S-PPZ and S-PPT membranes were 3976 and 2117, achieved at 60 °C and 40 °C, respectively. This indicates that the membrane structure at 40 °C effectively differentiates between water and ethanol molecules, likely due to a balanced interaction between water adsorption and ethanol rejection. As the temperature rises, the separation factor decreases slightly, likely due to increased ethanol permeation resulting from enhanced molecular mobility [42]. Despite this decline in selectivity, the PSI for the S-PPZ membrane reached a peak of 3976 at 60 °C, demonstrating that higher temperatures improve overall performance by increasing flux, even with a moderate loss in selectivity.

In comparison to other studies focusing on nano-composite membranes for pervaporation processes, where a trade-off effect often occurs between flux and separation factor, our modified PSf/PMMA composite membranes demonstrated superior performance. For instance, Vane et al. [43] developed a ZSM-5/PDMS membrane with a separation factor of 30 and a flux of 0.232 kg m^{-2} h^{-1}. Zhang et al. [44] reported a PDMS-based membrane with a separation factor of 7.6 and a total flux of 1.5 kg m^{-2} h^{-1} at an operating temperature of 70 °C. Zong et al. [45] achieved a relatively high flux of 2.4 kg m^{-2} h^{-1} with a moderate separation factor of 8.6 for their PDMS/PTFE composite membrane. Based on a comprehensive review of previous studies, our modified PSf/PMMA composite membranes in this study demonstrated comparatively better overall performance.

3.8 Permeate flux

Fig. 9 illustrates the impact of feed temperature on membrane performance, assessed through flux and separation factor values. Overall, the S-PPZ membrane exhibited higher flux and separation factor values compared to those with TiO_2 filler, achieving a maximum flux of 116.86 L m^{-2} h^{-1} at 70 °C and the highest separation factor of 60.17 at 40 °C. This observation is supported by the cross-sectional structures of the S-PPZ and S-PPT membranes. The S-PPZ membrane displays macro-voids that enhance its porosity, thereby increasing permeate flux. The relationship between membrane porosity and

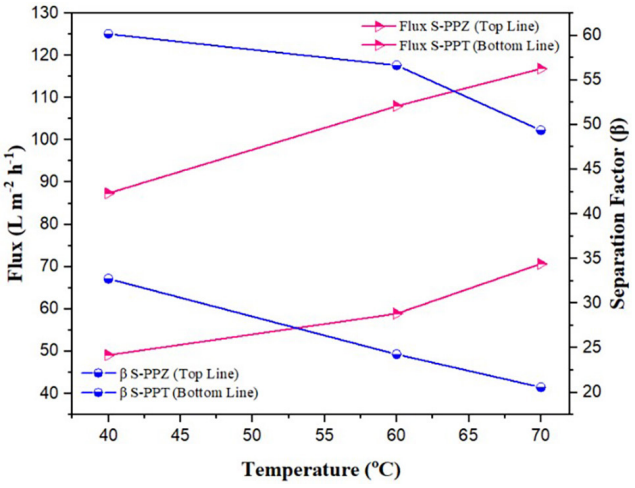

Fig. 9 Separation factor and permeate flux index of S-PPZ and S-PPT at different operating temperature

hydrophilicity is essential, increased porosity enhances hydrophilicity, which subsequently facilitates higher permeate flux. The more hydrophilic nature of the S-PPZ membrane results in significantly higher permeate flux compared to the S-PPT membrane. Fig. 9 also indicates that permeate flux increases with rising feed temperature for both membrane types. However, the separation factor decreases as the feed temperature increases. This increase in permeate flux, accompanied by a reduction in the separation factor, can be attributed to the thermal motion of feed components and polymer chains within the membrane [46]. Generally, temperature influences the transport behavior of permeates and facilitates the swelling of polymer chains within the membrane structure. At elevated temperatures, the frequency and amplitude of segmental motion in the polymer chains increase, leading to an increase in the volume of free space and a decrease in the degree of swelling of the polymer matrix. This increase in void volume allows for more efficient permeate transfer. Additionally, the vapor pressure of permeate molecules rises at higher temperatures. The combined effects of increased void volume and driving forces from the differences in vapor pressure result in higher flux and lower separation factor at elevated temperatures, allowing for greater diffusion of both ethanol and water molecules through the membrane [47].

3.9 Comparation with previous studies

In previous studies, polysulfone-based membranes have been widely investigated for their application in ethanol dehydration due to their promising properties, including chemical resistance and mechanical stability. Researchers have explored various modifications to PSf membranes to enhance their separation performance. Modifications such as the incorporation of inorganic fillers (e.g., zeolites, silica, and MOFs) and surface functionalization techniques have been reported to improve water permeation and ethanol rejection rates. The current study builds upon this foundation by focusing on PV-modified PSf membranes, evaluating their performance in ethanol dehydration compared to these previously reported materials (Table 3 [48–51]).

Table 3 Comparation with previous studies

Material	PSI (kg/m^2 h)	Separation factor	Ref.
PDMS-PTFPMS	13	11.3	[48]
MOF ZIF 8	78	300	[49]
SCMC-PDDA/PSf	8.26	612	[50]
PECSM-20/PSf	21.67	1570	[51]
PSf/PMMA/ZSM-5/TiO_2	3979	61.227	Present study

4 Conclusion

Successfully fabricated nano-composite PDMS-coated membranes comprising PSf/PMMA/ZSM-5 or TiO_2 for the pervaporation process have been developed. Morphological characterizations have verified the effective embedding of ZSM-5 nanocrystals and TiO_2 nanoparticles within the PSf/PMMA matrix. Moreover, the resulting nano-composite membranes exhibited a dense and uniform distribution of nanofillers. The incorporation and dispersion of ZSM-5 nanocrystals and TiO_2 nanoparticles into the PSf/PMMA membrane notably enhanced the physicochemical properties of the pervaporation membrane. The introduction of ZSM-5 or TiO_2 led to improved membrane hydrophilicity and mechanical properties. Overall, the membrane incorporating ZSM-5 demonstrated superior performance compared to TiO_2, showing a 2.2 times total flux enhancement. The nano-composite membrane with 2 wt.% ZSM-5 loading and PDMS coating achieved a PSI value of 3979 kg m^{-2} h^{-1}, along with a comparable separation factor of 61.22 at 40 °C. This high-performance PDMS-coated PSf/PMMA/ZSM-5 nano-composite membrane exhibits significant potential for ethanol permselective pervaporation applications.

Acknowledgement

The authors gratefully acknowledge the financial support of the Institute of Research and Community Services Universitas Diponegoro, Indonesia under International Publication Research Program Scheme No. 569-163/UN7. D2/PP/V/2023.

References

[1] Rehman, E., Rehman, S. "Modeling the nexus between carbon emissions, urbanization, population growth, energy consumption, and economic development in Asia: Evidence from grey relational analysis", Energy Reports, 8, pp. 5430–5442, 2022. https://doi.org/10.1016/j.egyr.2022.03.179

[2] Qyyum, M. A., Qadeer, K., Lee, M. "Comprehensive Review of the Design Optimization of Natural Gas Liquefaction Processes: Current Status and Perspectives", Industrial & Engineering Chemistry Research, 57(17), pp. 5819–5844, 2018. https://doi.org/10.1021/acs.iecr.7b03630

[3] Khalid, A., Aslam, M., Qyyum, M. A., Faisal, A., Khan, A. L., Ahmed, F., ..., Yasin, M. "Membrane separation processes for dehydration of bioethanol from fermentation broths: Recent developments, challenges, and prospects", Renewable and Sustainable Energy Reviews, 105, pp. 427–443, 2019. https://doi.org/10.1016/j.rser.2019.02.002

[4] Lee, Y. H., Chen, C. H., Umi Fazara, M. A., Irfan Hatim, M. D. M. "Production of fuel grade anhydrous ethanol: a review", IOP Conference Series: Earth and Environment Science, 765(1), 012016, 2021. https://doi.org/10.1088/1755-1315/765/1/012016

[5] Martins, F., Felgueiras, C., Smitkova, M., Caetano, N. "Analysis of Fossil Fuel Energy Consumption and Environmental Impacts in European Countries", Energies, 12(6), 964, 2019. https://doi.org/10.3390/en12060964

[6] Pillot, B., Muselli, M., Poggi, P., Dias, J. B. "Historical trends in global energy policy and renewable power system issues in Sub-Saharan Africa: The case of solar PV", Energy Policy, 127, pp. 113–124, 2019. https://doi.org/10.1016/j.enpol.2018.11.049

[7] Periyasamy, S., Beula Isabel, J., Kavitha, S., Karthik, V., Mohamed, B. A., Gizaw, D. G., Sivashanmugam, P., Aminabhavi, T. M. "Recent advances in consolidated bioprocessing for conversion of lignocellulosic biomass into bioethanol – A review", Chemical Engineering Journal, 453, 139783, 2023. https://doi.org/10.1016/j.cej.2022.139783

[8] Karin, P., Tripatara, A., Wai, P., Oh, B.-S., Charoenphonphanich, C., Chollacoop, N., Kosaka, H. "Influence of ethanol-biodiesel blends on diesel engines combustion behavior and particulate matter physicochemical characteristics", Case Studies in Chemical and Environmental Engineering, 6, 100249, 2022. https://doi.org/10.1016/j.cscee.2022.100249

[9] Sinha, S., Tripathi, P. "Trends and challenges in valorisation of food waste in developing economies: A case study of India", Case Studies in Chemical and Environmental Engineering, 4, 100162, 2021. https://doi.org/10.1016/j.cscee.2021.100162

[10] Zhang, H., Zhang, P., Wu, T., Ruan, H. "Bioethanol Production Based on *Saccharomyces cerevisiae*: Opportunities and Challenges", Fermentation, 9(8), 709, 2023. https://doi.org/10.3390/fermentation9080709

[11] Ruocco, C., Cortese, M., Martino, M., Palma, V. "Fuel grade bioethanol reforming in a fluidized bed reactor over highly durable Pt-Ni/CeO_2-SiO_2 catalysts", Chemical Engineering and Processing - Process Intensification, 174, 108888, 2022. https://doi.org/10.1016/j.cep.2022.108888

[12] Kusworo, T. D., Yulfarida, M., Kumoro, A. C., Utomo, D. P. "Purification of bioethanol fermentation broth using hydrophilic PVA crosslinked PVDF-GO/TiO_2 membrane", Chinese Journal of Chemical Engineering, 55, pp. 123–136, 2023. https://doi.org/10.1016/j.cjche.2022.04.028

[13] Kulkarni, A. S., Sajjan, A. M., M, A., Banapurmath, N. R., Ayachit, N. H., Shirnalli, G. G. "Novel fabrication of PSSAMA_Na capped silver nanoparticle embedded sodium alginate membranes for pervaporative dehydration of bioethanol", RSC Advances, 10(38), pp. 22645–22655, 2020. https://doi.org/10.1039/D0RA01951H

[14] Botshekan, M., Moheb, A., Vatankhah, F., Karimi, K., Shafiei, M. "Energy saving alternatives for renewable ethanol production with the focus on separation/purification units: A techno-economic analysis", Energy, 239, 122363, 2022. https://doi.org/10.1016/j.energy.2021.122363

[15] Mansy, A. E., El Desouky, E. A., Taha, T. H., Abu-Saied, M. A., El-Gendi, H., Amer, R. A., Tian, Z.-Y. "Sustainable production of bioethanol from office paper waste and its purification via blended polymeric membrane", Energy Conversion and Management, 299, 117855, 2024. https://doi.org/10.1016/j.enconman.2023.117855

[16] Sajjan, A. M., Premakshi, H. G., Kariduraganavar, M. Y. "Synthesis and characterization of polyelectrolyte complex membranes for the pervaporation separation of water–isopropanol mixtures using sodium alginate and gelatin", Polymer Bulletin, 75(2), pp. 851–875, 2018. https://doi.org/10.1007/s00289-017-2062-7

[17] Kalahal, P. B., Sajjan, A. M., Yunus Khan, T. M., Rajhi, A. A., Achappa, S., Banapurmath, N. R., M, A., Duhduh, A. A. "Novel Polyelectrolyte Complex Membranes Containing Carboxymethyl Cellulose–Gelatin for Pervaporation Dehydration of Azeotropic Bioethanol for Biofuel", Polymers, 14(23), 5114, 2022. https://doi.org/10.3390/polym14235114

[18] Si, Z., Liu, C., Xue, T., Yang, S., Cui, Y., Wang, Y., Cai, D., Qin, P. "Polymeric membranes through self-initiation and self-polymerization for high-performance bioethanol pervaporation", Journal of Materials Chemistry A, 10(34), pp. 17699–17709, 2022. https://doi.org/10.1039/D2TA04701B

[19] Sibeko, M. A., Saladino, M. L., Luyt, A. S., Caponetti, E. "Morphology and properties of poly(methyl methacrylate) (PMMA) filled with mesoporous silica (MCM-41) prepared by melt compounding", Journal of Materials Science, 51(8), pp. 3957–3970, 2016. https://doi.org/10.1007/s10853-015-9714-5

[20] Zainol Abidin, M. N., Goh, P. S., Said, N., Ismail, A. F., Othman, M. H. D., Hasbullah, H., …, Mansur, S. "Co-Adsorptive Removal of Creatinine and Urea by a Three-Component Dual-Layer Hollow Fiber Membrane", ACS Applied Materials & Interfaces, 12(29), pp. 33276–33287, 2020. https://doi.org/10.1021/acsami.0c08947

[21] Sardarabadi, H., Kiani, S., Karkhanechi, H., Mousavi, S. M., Saljoughi, E., Matsuyama, H. "Effect of Nanofillers on Properties and Pervaporation Performance of Nanocomposite Membranes: A Review", Membranes, 12(12), 1232, 2022. https://doi.org/10.3390/membranes12121232

[22] Weyd, M., Richter, H., Puhlfürß, P., Voigt, I., Hamel, C., Seidel-Morgenstern, A. "Transport of binary water–ethanol mixtures through a multilayer hydrophobic zeolite membrane", Journal of Membrane Science, 307(2), pp. 239–248, 2008. https://doi.org/10.1016/j.memsci.2007.09.032

[23] Chikkatti, B. S., Sajjan, A. M., Kalahal, P. B., Banapurmath, N. R., Angadi, A. R. "Insight into the performance of VRLA battery using PVA-TEOS hybrid gel electrolytes with titania nanoparticles", Journal of Energy Storage, 72, 108572, 2023. https://doi.org/10.1016/j.est.2023.108572

[24] Girão, A. V., Caputo, G., Ferro, M. C. "Chapter 6 - Application of Scanning Electron Microscopy–Energy Dispersive X-Ray Spectroscopy (SEM-EDS)", In: Rocha-Santos, T. A. P., Duarte, A. C. (eds.) Comprehensive Analytical Chemistry, vol. 75, Elsevier, 2017, pp. 153–168. ISBN 9780444638984 https://doi.org/10.1016/bs.coac.2016.10.002

[25] Lekoane, T., Msomi, P. F. "Quarternized polysulfone/ZSM-5 zeolite composite anion exchange membrane separators for aluminum-air battery", Journal of Applied Polymer Science, 140(27), e54006, 2023. https://doi.org/10.1002/app.54006

[26] Sagadevan, S., Chowdhury, Z. Z., Rafique, R. F. "Preparation and Characterization of Nickel ferrite Nanoparticles via Co-precipitation Method", Materials Research, 21(2), e20160533, 2018. https://doi.org/10.1590/1980-5373-mr-2016-0533

[27] Kusworo, T. D., Ariyanti, N., Utomo, D. P. "Effect of nano-TiO_2 loading in polysulfone membranes on the removal of pollutant following natural-rubber wastewater treatment", Journal of Water Process Engineering, 35, 101190, 2020. https://doi.org/10.1016/j.jwpe.2020.101190

[28] Li, X., Janke, A., Formanek, P., Fery, A., Stamm, M., Tripathi, B. P. "High permeation and antifouling polysulfone ultrafiltration membranes with *in situ* synthesized silica nanoparticles", Materials Today Communications, 22, 100784, 2020. https://doi.org/10.1016/j.mtcomm.2019.100784

[29] Misdan, N., Lau, W. J., Ismail, A. F., Matsuura, T., Rana, D. "Study on the thin film composite poly(piperazine-amide) nanofiltration membrane: Impacts of physicochemical properties of substrate on interfacial polymerization formation", Desalination, 344, pp. 198–205, 2014. https://doi.org/10.1016/j.desal.2014.03.036

[30] Kusworo, T. D., Ismail, A. F., Aryanti, N., Widayat, W., Qudratun, Q., Utomo, D. P. "Enhanced Anti-fouling Behavior and Performances of Nano Hybrid PES-SiO_2 and PES-ZnO Membranes for Produced Water Treatment", Jurnal Teknologi, 79(6), pp. 129–140, 2017. https://doi.org/10.11113/jt.v79.10692

[31] Alias, S. S., Harun, Z., Shohur, M. F. "Effect of monovalent and divalent ions in non-solvent coagulation bath-induced phase inversion on the characterization of a porous polysulfone membrane", Polymer Bulletin, 76(11), pp. 5957–5979, 2019. https://doi.org/10.1007/s00289-019-02689-z

[32] Lou, L., Kendall, R. J., Smith, E., Ramkumar, S. S. "Functional PVDF/rGO/TiO_2 nanofiber webs for the removal of oil from water", Polymer, 186, 122028, 2020. https://doi.org/10.1016/j.polymer.2019.122028

[33] Liu, Q., Xiao, T., Geng, L., Liu, C. "In situ encapsulation of phase change material by synergistic interaction of polymethyl methacrylate and nano-TiO_2", Journal of Energy Storage, 67, 107633, 2023. https://doi.org/10.1016/j.est.2023.107633

[34] Kocakulak, T., Taşkın, G., Tabanlıgil Calam, T., Solmaz, H., Calam, A., Arslan, T. A., Şahin, F. "A new nanocomposite membrane based on sulfonated polysulfone boron nitride for proton exchange membrane fuel cells: Its fabrication and characterization", Fuel, 374, 132476, 2024. https://doi.org/10.1016/j.fuel.2024.132476

[35] Plouzeau, M., Piogé, S., Peilleron, F., Fontaine, L., Pascual, S. "Polymer/dye blends: Preparation and optical performance: A short review", Journal of Applied Polymer Science, 139(36), e52861, 2022. https://doi.org/10.1002/app.52861

[36] Nasiri, S., Rabiei, M., Palevicius, A., Janusas, G., Vilkauskas, A., Nutalapati, V., Monshi, A. "Modified Scherrer equation to calculate crystal size by XRD with high accuracy, examples Fe_2O_3, TiO_2 and V_2O_5", Nano Trends, 3, 100015, 2023. https://doi.org/10.1016/j.nwnano.2023.100015

[37] Xu, Z., Wu, T., Shi, J., Teng, K., Wang, W., Ma, M., Li, J., Qian, X., Li, C., Fan, J. "Photocatalytic antifouling PVDF ultrafiltration membranes based on synergy of graphene oxide and TiO_2 for water treatment", Journal of Membrane Science, 520, pp. 281–293, 2016. https://doi.org/10.1016/j.memsci.2016.07.060

[38] Wang, Y., Yan, L., Ling, Y., Ge, Y., Huang, C., Zhou, S., Xia, S., Liang, M., Zou, H. "Enhanced mechanical and adhesive properties of PDMS coatings via in-situ formation of uniformly dispersed epoxy reinforcing phase", Progress in Organic Coatings, 174, 107319, 2023. https://doi.org/10.1016/j.porgcoat.2022.107319

[39] Zhan, X., Lu, J., Tan, T., Li, J. "Mixed matrix membranes with HF acid etched ZSM-5 for ethanol/water separation: Preparation and pervaporation performance", Applied Surface Science, 259, pp. 547–556, 2012. https://doi.org/10.1016/j.apsusc.2012.05.167

[40] He, X., Wang, T., Huang, J., Chen, J., Li, J. "Fabrication and characterization of superhydrophobic PDMS composite membranes for efficient ethanol recovery via pervaporation", Separation and Purification Technology, 241, 116675, 2020. https://doi.org/10.1016/j.seppur.2020.116675

[41] Dave, H. K., Nath, K. "Effect of Temperature on Pervaporation Dehydration of Water-Acetic Acid Binary Mixture", Journal of Scientific & Industrial Research, 76, pp. 217–222, 2017.

[43] Vane, L. M., Namboodiri, V. V., Bowen, T. C. "Hydrophobic zeolite–silicone rubber mixed matrix membranes for ethanol–water separation: Effect of zeolite and silicone component selection on pervaporation performance", Journal of Membrane Science, 308(1–2), pp. 230–241, 2008. https://doi.org/10.1016/j.memsci.2007.10.003

[44] Zhang, G., Li, J., Wang, N., Fan, H., Zhang, R., Zhang, G., Ji, S. "Enhanced flux of polydimethylsiloxane membrane for ethanol permselective pervaporation via incorporation of MIL-53 particles", Journal of Membrane Science, 492, pp. 322–330, 2015. https://doi.org/10.1016/j.memsci.2015.05.070

[45] Zong, C., Yang, X., Chen, D., Chen, Y., Zhou, H., Jin, W. "Rational tuning of the viscosity of membrane solution for the preparation of sub-micron thick PDMS composite membrane for pervaporation of ethanol-water solution", Separation and Purification Technology, 255, 117729, 2021. https://doi.org/10.1016/j.seppur.2020.117729

[46] Ong, Y. K., Shi, G. M., Le, N. L., Tang, Y. P., Zuo, J., Nunes, S. P., Chung, T.-S. "Recent membrane development for pervaporation processes", Progress in Polymer Science, 57, pp. 1–31, 2016. https://doi.org/10.1016/j.progpolymsci.2016.02.003

[47] Vane, L. M. "Review of pervaporation and vapor permeation process factors affecting the removal of water from industrial solvents", Journal of Chemical Technology and Biotechnology, 95(3), pp. 495–512, 2020.
https://doi.org/10.1002/jctb.6264

[48] Liu, C., Xue, T., Yang, Y., Ouyang, J., Chen, H., Yang, S., Li, G., Cai, D., Si, Z., Li, S., Qin, P. "Effect of crosslinker 3-methacryloxypropylmethyldimethoxysilane on UV-crosslinked PDMS-PTFPMS block copolymer membranes for ethanol pervaporation", Chemical Engineering Research and Design, 168, pp. 13–24, 2021.
https://doi.org/10.1016/j.cherd.2021.01.023

[49] Kudasheva, A., Sorribas, S., Zornoza, B., Téllez, C., Coronas, J. "Pervaporation of water/ethanol mixtures through polyimide based mixed matrix membranes containing ZIF-8, ordered mesoporous silica and ZIF-8-silica core-shell spheres", Journal of Chemical Technology and Biotechnology, 90(4), pp. 669–677, 2015.
https://doi.org/10.1002/jctb.4352

[50] Wang, X.-S., An, Q.-F., Zhao, Q., Lee, K.-R., Qian, J.-W., Gao, C.-J. "Homogenous polyelectrolyte complex membranes incorporated with strong ion-pairs with high pervaporation performance for dehydration of ethanol", Journal of Membrane Science, 435, pp. 71–79, 2013.
https://doi.org/10.1016/j.memsci.2013.02.008

[51] Wang, X.-S., An, Q.-F., Liu, T., Zhao, Q., Hung, W.-S., Lee, K.-R., Gao, C.-J. "Novel polyelectrolyte complex membranes containing free sulfate groups with improved pervaporation dehydration of ethanol", Journal of Membrane Science, 452, pp. 73–81, 2014.
https://doi.org/10.1016/j.memsci.2013.10.028